

# Influence of ENSO and SAM on the occurrence of absolute extremes and behavior of Ta, SST, and SIC anomalies in the western Antarctic Peninsula

Daniela MONTAÑO BELLO<sup>1\*</sup> and Nancy Liliana VILLEGAS BOLAÑOS<sup>2</sup>

<sup>1</sup> Grupo de Estudios en Asuntos Antárticos. Departamento de Geociencias, Universidad Nacional de Colombia, Bogotá D.C., 111321, Colombia.

<sup>2</sup> Grupo de Investigación en Oceanología CENIT. Departamento de Geociencias, Universidad Nacional de Colombia, Bogotá D.C., 111321, Colombia.

\*Corresponding author; email: dmontanob@unal.edu.co

Received: August 16, 2024; Accepted: March 4, 2025

## RESUMEN

El objetivo de este trabajo es mejorar la comprensión de la interacción entre los eventos de El Niño-Oscilación del Sur (ENOS) y las fases de la Oscilación Antártica (OAA), así como su influencia en el oeste de la Península Antártica (OPA). Se utilizaron series mensuales de temperatura del aire (Ta), temperatura superficial del mar (TSM) y cobertura de hielo marino (CHM) del periodo 1981-2020 para seis puntos representativos de la región de estudio. Los datos de Ta, CHM y TSM fueron obtenidos de la base de datos ERA5. Los índices de la Oscilación del Sur (IOS) y la Oscilación Antártica (IOAA) fueron extraídos del Centro de Predicción del Clima de la NOAA. Se realizó el cálculo de la densidad espectral de las series de anomalías de cada variable y su descomposición en ciclos característicos de la OAA y el ENOS. Se identificaron los componentes más influyentes en las oscilaciones de las series de estudio. Se llevó a cabo un análisis de correlación cruzada entre las componentes de las anomalías de Ta, CHM y TSM, y los índices IOS y IOAA. Se encontró que las series de Ta presentan correlaciones positivas y moderadas con la OAA, particularmente entre el cuasiperiodo de 5.2 años del IOAA y el cuasiperiodo de 4.4 años de Ta para el Paso de Drake y el Estrecho de Bransfield. Las series de TSM en Bransfield se correlacionan con el IOAA5.2, mientras que los cuasiperiodos de 4.6 y 5.2 años en el Paso de Drake se correlacionan con el IOS3.5. Las series de CHM muestran correlaciones positivas con el cuasiperiodo de 3.5 años del IOS cuando los rezagos son superiores a un año, excepto en el Estrecho de Bransfield. Los eventos extremos de Ta y TSM en la región OPA están fuertemente influenciados por la OAA y el ENOS. Se concluye que el acoplamiento de las fases del ENOS y la OAA amplifica los efectos sobre las variables meteo-marinas.

## ABSTRACT

This study aims to improve the understanding of the interaction between El Niño-Southern Oscillation (ENSO) events and the phases of the Southern Annular Mode (SAM), as well as their influence on the western Antarctic Peninsula (WAP). Monthly series of air temperature (Ta), sea surface temperature (SST), and sea ice coverage (SIC) from 1981 to 2020 were analyzed at six representative points within the study area. Ta, SIC, and SST data were obtained from the ERA5 database. The Southern Oscillation Index (SOI) and Antarctic Oscillation Index (AAOI) were sourced from NOAA's Climate Prediction Center. The spectral density of the anomaly series for each variable was calculated, and the characteristic cycles of SAM and ENSO were extracted. The most influential components driving the oscillations of the studied series were identified. A cross-correlation analysis was conducted between the anomaly components of Ta, SIC, and SST and those of SOI and AAOI. The results indicate that Ta series exhibit moderate positive correlations with SAM, particularly between the 5.2-year quasi-period of AAOI and the 4.4-year quasi-period of Ta in the Drake Passage and Bransfield Strait. The SST series in Bransfield correlate with AAOI5.2, while the quasi-periods of 4.6

and 5.2 years in the Drake Passage correlate with SOI3.5. The SIC series show positive correlations with the 3.5-year quasi-period of SOI for lag times greater than one year, except in the Bransfield Strait. Extreme absolute  $T_a$  and SST events in the WAP region are strongly influenced by SAM and ENSO. It is concluded that the coupling of ENSO and SAM phases amplifies their effects on meteo-marine variables.

**Keywords:** ERA5, correlation, spectral density, Bransfield, Gerlache.

## 1. Introduction

Polar regions, such as the Arctic and Antarctic, play a crucial role in ocean dynamics, as they are key areas where warm water currents undergo cooling. The Southern Ocean (Antarctic) serves as the primary link between the Atlantic, Pacific, and Indian oceans, making it a fundamental component of global circulation. Consequently, processes occurring in Antarctica have a significant impact on the global climate and are particularly sensitive to variability and climate change. In particular, the western part of the Antarctic Peninsula (WAP) has experienced a marked increase in air temperature ( $T_a$ ) and sea surface temperature (SST) over the past 50 years (Cook et al., 2016; Stenni et al., 2017).

Climatology in the Southern Hemisphere is primarily influenced by the Southern Annular Mode (SAM), which drives atmospheric pressure variations between 65° S in Antarctica and 40° S in South America, defining two distinct phases (Pohl et al., 2010). During the positive SAM phase, westerly winds intensify and shift poleward, whereas in the negative SAM phase, they weaken and move equatorward (Fogt and Marshall, 2020). Another key factor shaping the region's climatology is the El Niño-Southern Oscillation (ENSO). According to Meredith et al. (2008), the southeastern Pacific, particularly the area near the Antarctic Peninsula, is highly sensitive to ENSO forcing due to anomalous meridional winds. As a result, extreme events and anomalies in meteorological and oceanic parameters in the WAP region may be directly linked to the phases of these climate variability patterns.

Numerous studies have explored the relationship between SST behavior and the SAM. Spence et al. (2014) conducted simulations using the Modular Ocean Model (MOM), applying a wind perturbation along the west coast with a positive phase of SAM. Their findings suggest that WAP warming results from an anomalous intrusion of warm circumpolar

deep waters onto the continental shelf. This occurs in response to reduced Ekman pumping in coastal surface waters, caused by changes in local wind patterns. Later, the same authors performed new simulations, this time applying the perturbation along the east coast of Antarctica. They assert that barotropic Kelvin waves, trapped along the coast, propagate the wind disturbance along the Antarctic coastline. In the WAP region, circulation is further intensified by the continental slope and the presence of pre-existing warm subsurface waters. These factors contribute to the observed warming in the WAP (Spence et al., 2017).

According to Dotto et al. (2016), during a positive SAM phase, the interaction of water masses between the Bransfield Strait and the Weddell Sea is reduced. In contrast, during the negative SAM phase, there is an increase in water inflow from the Weddell Sea. This is due to the northward shift of the wind belt, ocean fronts, and more intense coastal currents in the Weddell Sea. Likewise, Ruiz et al. (2018) found that during La Niña phases, the modified Circumpolar Deep Water (CDW) core extended along the southern slope of the South Shetland Islands. Conversely, in El Niño phases, the core was partially or entirely absent. Additionally, since the 2000s, a southward extension of the CDW core has been recorded within the western basin of Bransfield Strait, possibly associated with positive SAM phases.

Furthermore, Wang et al. (2022) describe a seasonal cycle of coastal transport in which, during winter, there is a net flow of cold water into the central WAP. This pattern reverses in summer, bringing a net flow of CDW and its modified form into the Bransfield Strait. They also found that wind forcing modulates the trajectory of a coastal current carrying Weddell water along the WAP shelf. In winters with a positive SAM phase, stronger upwelling-favorable winds in the Bransfield Strait drive the offshore advection of Weddell water. Conversely, during a negative SAM

phase, weaker upwelling or downwelling winds allow more cold water from the Bransfield Strait to flood the WAP.

Other studies associate ENSO and SAM with deep waters intrusions into the Bransfield Strait. Damini et al. (2022) reported that ENSO affects both the intensity and frequency of northwesterly winds in the region. During negative phases, northwesterly winds strengthen and become more frequent, shifting the Southern ACC Front (SACCF) and Southern Boundary (SB) currents toward the Antarctic Peninsula. As a result, CDW inflow into the Bransfield Strait intensifies. In contrast, during the positive ENSO phases, northerly winds in the western Antarctic Peninsula weaken and become less frequent. This shifts the SACCF and SB northward, reducing CDW inflow. Additionally, when both modes coincide (such as La Niña with positive SAM or El Niño with negative SAM), there is an increase (decrease) in CDW advection into the Bransfield Strait, associated with a decrease (increase) in the transport of surface waters along the western Antarctic Peninsula (Ruiz et al., 2018).

Evtushevsky et al. (2021) identified a 16-year periodicity in the air temperature of the Antarctic Peninsula, primarily in its northern region, closely correlated with pressure anomalies in the southwestern Atlantic linked to quasi-stationary extratropical waves and SAM. This finding suggests that atmospheric processes play a more significant role than oceanic processes in this interdecadal variability. They also observed that variability in the coupling between ENSO and SAM leads to regional circulation anomalies, which in turn generate differences in winter climate variability across different areas of the Antarctic Peninsula. This occurs through the redistribution of zonal and meridional flows and the predominant advection of warm or cold air. Recently, Suryawanshi et al. (2023) associated the observed decline in sea ice between 2016 and 2022 with the intensification of atmospheric zonal waves, highlighting a shift in the Interdecadal Pacific Oscillation and a positive phase of SAM during this period. Understanding how these climatic variability processes influence meteorological and oceanographic variables is crucial for predicting extreme events. In this context, the present study aims to identify the relationship between anomalies and absolute extreme events of Ta, SST, and SIC in relation to

ocean-atmosphere interaction processes, specifically ENSO and SAM.

## 2. Study area

The WAP oceanic region is divided into two main areas: the Bransfield Strait and the central WAP. The Bransfield Strait is an elongated basin parallel to the coast, with depths exceeding 2000 m. It is bounded by the South Shetland Islands to the northwest and the Boyd Strait to the south. The central WAP, located between Low Island and Alexander Island (71° S, 70° W), features typical depths of approximately 400 m and several depressions that extend across the shelf, deepening toward the coast (Moffat and Meredith, 2018). The study area spans latitudes 60°-66° S and longitudes 57°-67° W (Fig. 1). The circulation in the Bransfield Strait is dominated by a cyclonic gyre, with a branch flowing southwest around the tip of the peninsula, transporting cold Weddell Sea water toward the peninsula's coastal front (von Gyldenfeldt et al., 2002). In the central WAP, the hydrography is strongly influenced by air-sea interactions, the availability of CDW along the shelf slope, and ice melt (Moffat and Meredith, 2018).

Regarding meteorological conditions, the Antarctic Peninsula intersects with the Circumpolar Trough (CPT), a region of low pressure encircling the continent. Consequently, the central and northern sectors of the peninsula are influenced by strong westerly winds prevailing north of the trough, while easterly coastal winds dominate in the southern part of the region. It is important to note that the CPT is not perfectly symmetrical, as it contains climatological low-pressure centers. One of the most significant is the Amundsen Sea Low (ASL) system (Raphael et al., 2016), which causes the dominant winds along the west coast to originate primarily from the northwest rather than directly from the west. This facilitates the advection of relatively warm mid-latitude air masses into the region, making it warmer compared to other regions at similar latitudes. The contrasting low-level wind regimes, shaped by the orographic barrier of the mountain range, result in an annual mean air temperature on the west coast about 5-10 °C higher than at comparable latitudes on the east coast (Morris and Vaughan, 2003). These climate differences between the east and west coasts of the peninsula are further

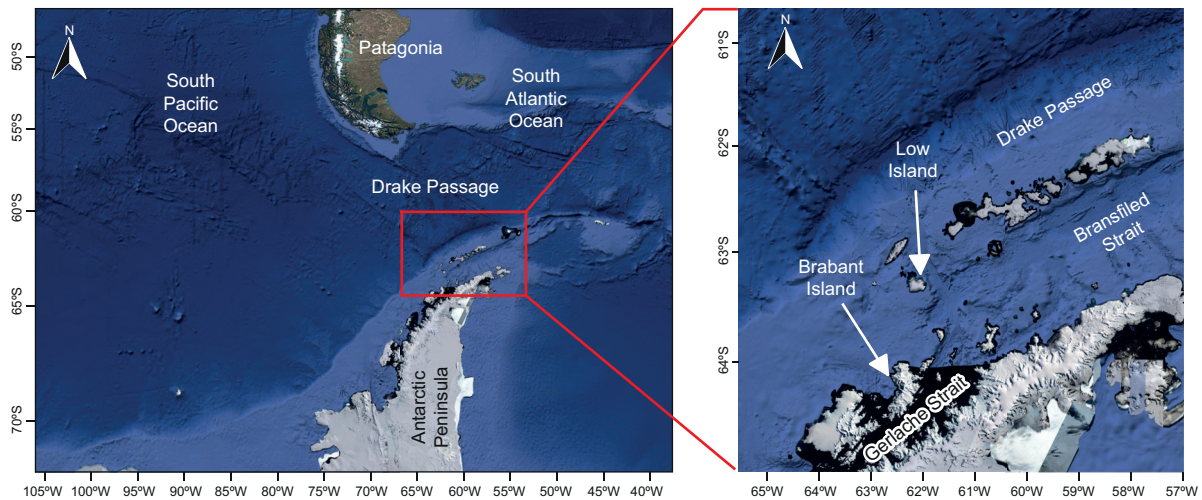


Fig. 1. Study area: Oceanic region of the western Antarctic Peninsula, located between 60°-66° S and 57°-67° W.

reinforced by the contrasting sea ice regimes on both sides (Domack et al., 2003).

The Antarctic Circumpolar Current (ACC) influences the distribution of salinity and temperature, creating pronounced gradients in adjacent areas. In the northern part of the region, within the Drake Passage, the ACC transports warmer waters from the north, resulting in relatively higher SST. The ACC interacts significantly with three major fronts: the Antarctic Slope Front (SAF), the Polar Front (PF), and the SACCF. These fronts play a crucial role in defining the boundaries and dynamics of the ACC. The SAF, located at the northern limit, marks the beginning of the current's circumpolar characteristics. The PF, situated further south, delineates the transition to colder and fresher Antarctic surface waters. Finally, the SACCF, positioned even farther south, represents the southern extension of the Circumpolar Deep Water (CDW) mass (Wu et al., 2019).

### 3. Methodology

Monthly data on air temperature ( $T_a$ , °C), sea ice concentration (SIC, 0-1), and sea surface temperature (SST, °C) for the period 1981-2020 were obtained from the ERA5 reanalysis, available through the Copernicus Climate Change Service (C3S) Climate Data Store (CDS) (Hersbach et al., 2020). Turner et al. (2019) and Bozkurt et al. (2020) demonstrated through inter-comparison studies that ERA5 and ERA-Interim data

reliably represent recent Antarctic climate conditions. Furthermore, Hernández et al. (2021) employed ERA5 data for sectors within this region, successfully describing the metocean conditions over the 1979-2018 period. Accordingly, ERA5 is used with confidence in the present study, without the need for additional validation. Additionally, the Antarctic Oscillation Index (AAOI) and the Southern Oscillation Index (SOI) were obtained from the NOAA Climate Prediction Center (NOAA-CPC, 2023).

A hierarchical cluster analysis was conducted to determine the optimal number of clusters, considering the multi-year annual mean of SST and sea surface salinity (SSS) obtained from the Ocean Reanalysis System 5 (ORAS5) (Balmaseda et al., 2013), along with their respective standard deviations at each 0.25° grid point. This analysis was performed using Statistica software (StatSoft, 2007), applying Ward's method (Ward, 1963) and Euclidean distance as the similarity measure. Through K-means clustering, the centroids of the homogeneous areas were identified, allowing the selection of six reference points (Fig. 2). Point 1 (63.5° S, 60° W) is located in the Bransfield Strait. Point 2 (64° S, 61.5° W) lies east of Brabant Island, influenced by nearby ice shelves and sea ice. Point 3 (64.5° S, 63° W) is in the Gerlache Strait. Point 4 (63.5° S, 62.75° W) is west of Low Island. Point 5 (61.75° S, 62.5° W) is north of Low Island. Finally, Point 6 (60.25° S, 57.75° W), is situated in the Drake Passage.

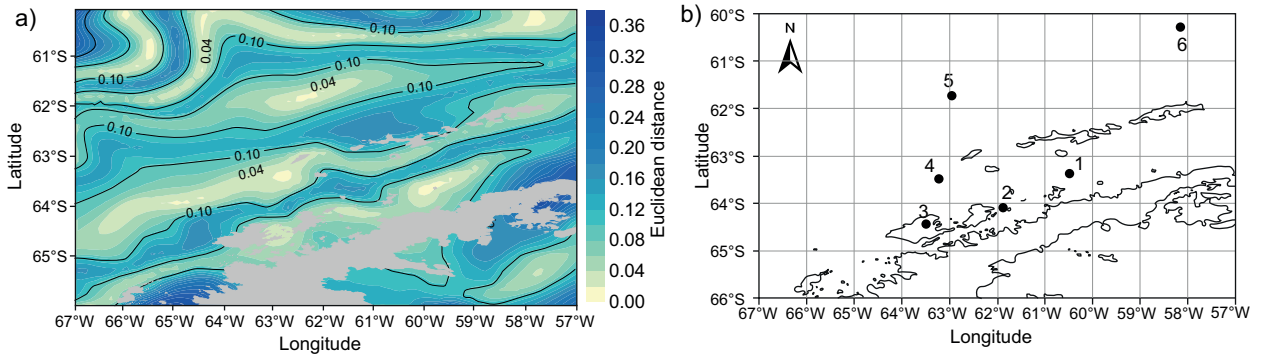


Fig. 2. (a) Distribution of Euclidean distances. The plot shows the variation in distances calculated during the clustering process, where smaller distances indicate a stronger match to the centroid, and larger distances suggest a weaker association. (b) Representative points selected: (1) 63.5° S, 60° W; (2) 64° S, 61.5° W; (3) 64.5° S, 63° W; (4) 63.5° S, 62.75° W; (5) 61.75° S, 62.5° W; (6) 60.25° S, 57.75° W.

Considering the base period 1981-2020, anomalies of  $T_a$ , SST, and SIC were calculated at the representative points. The anomaly series, along with the AAOI and SOI climatic indices, were decomposed by calculating spectral density using the AECPA software (Villegas and Malikov, 2020). This technique, employed in data analysis to break down a signal or function into its frequency components (Houser et al., 2022), is useful for characterizing dominant climate patterns in a time series, including seasonal, interannual, and decadal variations. Subsequently, a bandpass filter was applied with the AECPA software (Villegas and Malikov, 2020) to extract specific components at the time scales of interest while removing unwanted noise or variability. Finally, a cross-correlation analysis was performed to examine the connections between the original anomaly series and the extracted quasi-periods using the AECPA software (Villegas and Malikov, 2020). The significance level was set at 5% ( $p$ -value  $< 0.05$ ).

## 4. Results

### 4.1 Extreme absolute events of $T_a$ , SST, and SIC occurring during 1981-2020

The temporal evolution of  $T_a$ , SST, and SIC anomalies at the representative points of the study area is shown in panels a, b, and c of Figure 3, respectively. In general, the most pronounced negative  $T_a$  anomalies were observed before 1996 at all six analyzed points. Notably, P1, located in the Bransfield Strait, exhibits significant consecutive positive peaks in  $T_a$  anomalies

after 2008. Regarding SST, P1 predominantly exhibits negative anomalies until 2004, after which it becomes positive. P2, P3, and P4 show mainly negative anomalies before 1993, followed by positive peaks after 2008. P5 and P6, located in the Drake Passage, display a similar behavior to each other, differing from the other analyzed points. For SIC anomalies, P1 through P4 predominantly exhibit positive values before 2005, but then turn negative afterward. The open-ocean points (P5 and P6) show few negative anomalies, as expected given their lower sea ice coverage.

For the absolute extremes of  $T_a$  at the six reference points, nearly all exhibit the warmest event in July 1989, except for P4, located west of the South Shetland Islands and north of Brabant Island, where it occurred in August 2003. The absolute coldest  $T_a$  extreme was recorded in July 1987 at all points (Fig. 3a). Regarding SST extremes, the absolute warmest event occurred in January-February 2017 at the first four points, while for P5 it was in March 2006, and for P6 in February 2020. The absolute coldest SST extremes occurred in February 1987 at P4 and P5, in December 1986 at P2, in February 1982 at P3, and in February 2016 at P6 (Fig. 3b).

The absolute highest SIC extremes occurred in November 1986 at reference points P3 and P5, in July 1987 at P2 and P4, in December 1988 at P1, and in August 1995 at P6. Regarding the absolute lowest SIC extremes, P1 reached its minimum in August 2008, while P2 recorded minima in both August 2008 and 2010. For P3 and P4, the lowest SIC values occurred in September and August 1989,

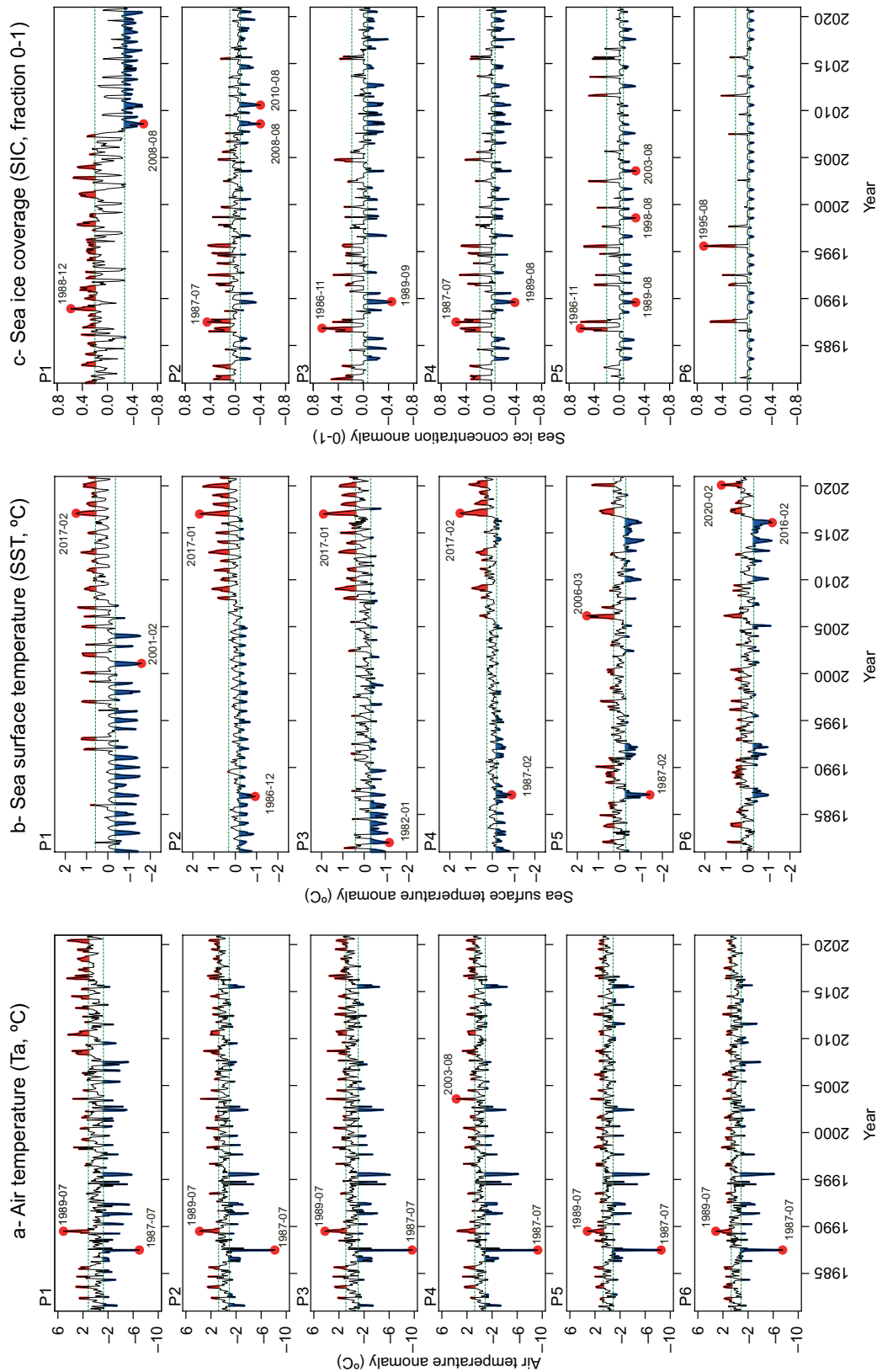


Fig. 3. Time series anomalies at reference points (1-6), calculated using the 1981-2020 climatological baseline. (a) Air temperature (Ta, °C); (b) sea surface temperature (SST, °C); and (c) sea ice coverage (SIC, fraction 0-1).

respectively. P5 showed three distinct minima: August 1989, 1998, and 2003. In contrast, P6, located in the northern part of the peninsula and in open sea, does not exhibit a clearly identifiable absolute minimum SIC event (Fig. 3c).

4.2 Quasi-periods extracted from the Ta, SST, and SIC series for the period 1981-2020

The spectral density calculated for the AAOI and SOI indices is presented in panels a and b of Figure 4, respectively. In these graphs, the x-axis represents the frequency, where period and frequency are reciprocal (e.g., a 15-month period corresponds to a frequency of 1/15 or 0.067 month<sup>-1</sup>). The AAOI periodogram reveals a series of distinct peaks rising above the background noise, indicating multiple periodic components that significantly contribute to the variability of the time series. Each peak represents a specific frequency associated with a recurring pattern or cycle in the AAOI. The dominant spectral components contributing to the variability of the AAOI correspond to cycles of approximately 2.2 and 5.2 years (Fig. 4a), both of which are statistically significant at the 5% level (p-value < 0.05). Similarly, the SOI periodogram displays two dominant spectral density peaks, indicating that its variability is primarily driven by cycles of approximately 2.4 and 3.5 years (Fig. 4b).

Periodograms of Ta, SST, and SIC anomalies at the representative points were prepared but are not included in this article. At P1, located in the Bransfield Strait, Ta and SST anomalies exhibit greater variability in frequencies and more pronounced peaks, while SIC anomalies show lower frequencies

compared to the other analyzed points. A summary of the quasi-periods is presented in Table I; these represent the approximate periods in years of the recurrent oscillations identified in the respective data series. The quasi-period of 4.4 years consistently appears across multiple Ta and SIC anomaly series. Likewise, quasi-periods of 1.0 and 0.8 years are recurrent in

Table I. Periods identified in the anomalies of air temperature (Ta, °C), sea surface temperature (SST, °C), and sea ice coverage (SIC, fraction 0-1) at reference points 1-6, based on spectral density analysis for the period 1981-2020.

Series analyzed	Quasi-periods (years)
Ta1	4.4; 1.0; 0.5
Ta2	4.4; 1.1; 0.8
Ta3	4.4; 1.3; 0.8
Ta4	4.4; 1.1; 0.5
Ta5	4.4; 1.1; 0.8; 0.5
Ta6	4.4; 2.4; 1.3; 0.8
SIC1	8.3; 3.1; 1.7
SIC2	3.6; 1.2; 0.8
SIC3	4.4; 1.2; 0.8
SIC4	4.6; 1.2; 0.8
SIC5	4.4; 2.8; 0.8
SIC6	4.4; 2.0; 1.3; 0.8
SST1	3.0; 1.7; 1.0
SST2	8.3; 1.0; 0.5
SST3	3.6; 1.0; 0.8
SST4	6.9; 1.0
SST5	4.6; 1.5; 0.9
SST6	5.2; 1.1; 0.9
SOI	3.5; 2.4
AAOI	5.2; 2.2

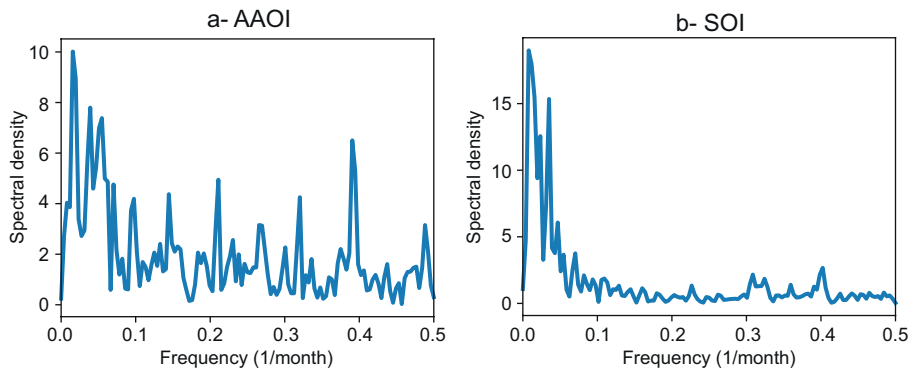


Fig. 4. Spectral density of (a) the Antarctic Oscillation Index (AAOI) and (b) the Southern Oscillation Index (SOI) during the period 1981-2020.

several series, indicating a shared frequency in climatic oscillations. Notably, an 8.3-year quasi-period appears only in the SIC1 and SST2 series, reflecting the dominant frequencies in the temporal behavior at each reference point.

Figure 5a shows the main cycles extracted from the AAOI index using a bandpass filter, corresponding to AAOI\_5.2 and AAOI\_2.2. Similarly, Figure 5b presents the main cycles extracted from the SOI index, corresponding to SOI\_3.5 and SOI\_2.4. The sum of components in each graph reveals that when the main index components are in phase, the signal is amplified. This occurs because in-phase variations contribute constructively, intensifying their effects.

These fluctuations are linked to changes in wind forcing, which are strongly influenced by coupled climatic variability modes and significantly impact the meridional winds in the WAP region.

#### 4.3 Cross-correlation between the original series and the extracted quasi-periods

The results of the cross-correlations between the original climatic series and the AAOI and SOI indices are presented in Table II. The air temperature series (Ta1 to Ta6) exhibit moderate positive correlations with the AAOI, ranging from 0.42 to 0.50 with no lag. In contrast, their correlations with the SOI are minimal, with coefficients ranging from 0.17 to 0.22.

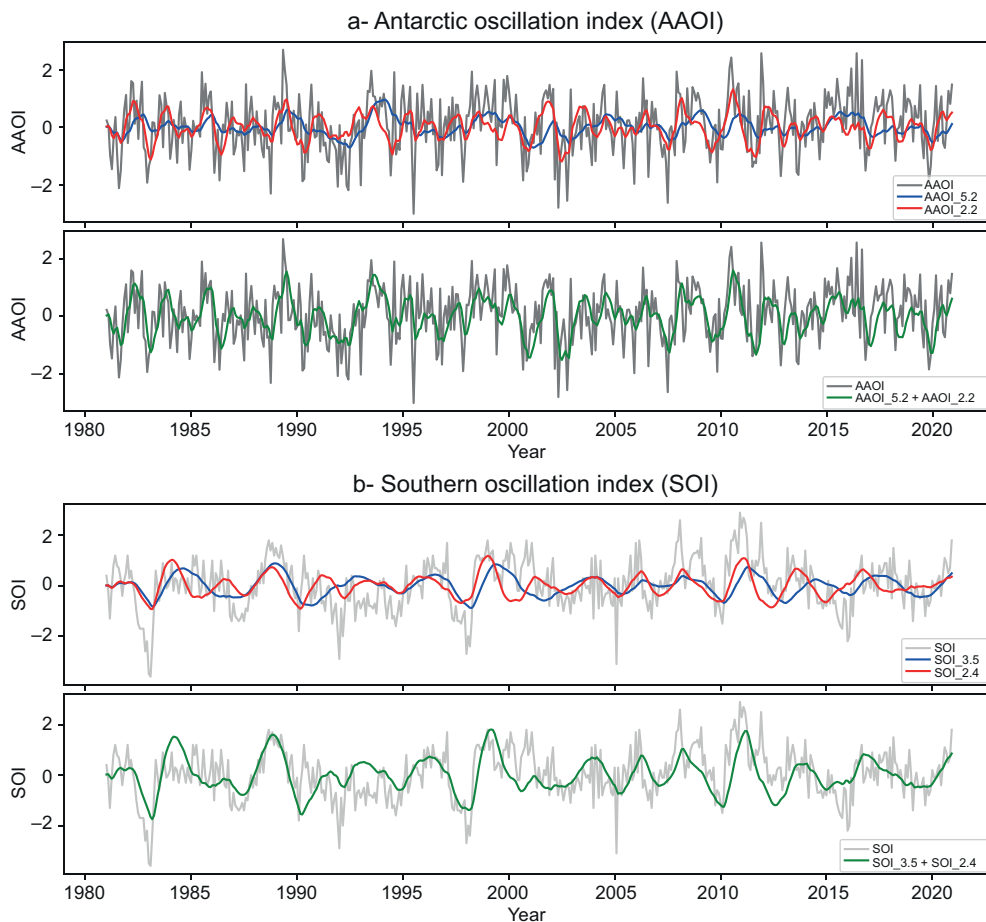


Fig. 5. Original series (gray curve) and main cycles extracted using a bandpass filter (red and blue curves, above), along with the sum of principal components (green curve, below) for (a) the Antarctic Oscillation Index (AAOI) and (b) the Southern Oscillation Index (SOI) during the period 1981-2020.

Table II. Cross-correlation coefficients between the original anomaly series of air temperature (Ta), sea surface temperature (SST), and sea ice concentration (SIC) at reference points 1-6, and the Antarctic Oscillation Index (AAOI) and Southern Oscillation Index (SOI) for the period 1981-2020.

Initial series	AAOI	SOI
Ta1	0.50(0)	0.17(-2)
Ta2	0.43(0)	0.21(2)
Ta3	0.42(0)	0.21(5)
Ta4	0.41(0)	0.22(2)
Ta5	0.42(0)	0.22(0)
Ta6	0.50(0)	0.21(0)
SIC1	-0.23(-1)	-0.18(1)
SIC2	-0.20(-2)	-0.25(3)
SIC3	-0.16(-2)	-0.27(3)
SIC4	-0.20(-1)	-0.24(3)
SIC5	-0.19(-1)	-0.19(5)
SIC6	-0.23(-1)	-0.13(-3)
SST1	0.16(17)	0.17(0)
SST2	0.14(0)	0.20(0)
SST3	0.15(-11)	0.13(10)
SST4	0.17(-1)	0.30(-3)
SST5	-0.14(15)	0.23(0)
SST6	0.17(-1)	0.27(-3)

Lag months are shown in parentheses; statistical significance at 5% ( $p$ -value < 0.05).

Furthermore, the SIC series (SIC1 to SIC6) exhibit negative correlations with both the AAOI and the SOI, with low correlation coefficients ranging from  $-0.16$  to  $-0.23$  for the AAOI and from  $-0.13$  to  $-0.27$  for the SOI. This indicates an inverse relationship between SIC and these climatic indices. Some of these correlations show lags of up to five months. Regarding the SST series (SST1 to SST6), both positive and negative correlations are observed. The correlation is weak, with coefficients ranging from  $-0.14$  to  $0.17$  for the AAOI, and from  $0.13$  to  $0.30$  with the SOI. Additionally, some of these correlations present lags of up to 17 months.

The summary of the cross-correlation and lags between the quasi-periods is shown in Table III, which includes only values greater than  $0.30$  in absolute terms. The lag months corresponding to the highest correlation value are indicated in parentheses. The most significant correlation observed was between

the 2.4-year component of Ta at P6 and the 2.4-year quasi-period of the SOI index, showing an inverse relationship with a coefficient of  $-0.60$  and a lag of 14 months.

The 4.4-year component of all Ta series exhibits a positive, moderate correlation with no lag to the 5.2-year quasi-period of the AAOI index. In contrast, the one-year component of the Ta2, Ta3, Ta4, and Ta5 series shows a negative, moderate correlation with a lag of five to six months. Additionally, a notable positive correlation greater than  $0.5$ , with no lag, is observed between the 2.2-year component of the AAOI and the one-year quasi-period of the Ta1 and Ta6 series. This highlights a strong association between Ta variability and AAOI oscillations.

Analyzing the correlation between the SOI3.5 index and air temperature, only the 4.4-year component of P6 exhibits a positive correlation with a three-month lag. In contrast, the other Ta series show negative correlations, with lags ranging from six to 16 months depending on the reference point. The shortest lag is observed at P4, which is located farther west and south and is not shielded by an orographic barrier that could obstruct westerly winds, unlike the other analyzed points.

Regarding SST, the 1.7-year component of SST1 shows a negative correlation of  $-0.31$  with the 5.2-year component of the AAOI index, with a 10 months lag. For the 4.6-year component of SST5, a stronger negative correlation is observed, reaching  $-0.41$  with a 15-month lag. The 1.5-year component of SST5 also exhibits a negative correlation of  $-0.33$  with the 2.2-year component of the AAOI index, with a 14-month lag. In the case of the 5.2-year component of SST6, two positive correlations are evident:  $0.30$  with the 5.2-year component of the AAOI index, with no lag, and  $0.47$  with the 3.5-year component of the SOI index, with a five-month lag.

In the case of SIC anomaly series, the 3.5-year component of the SOI index and the 3.6- and 4.4-year quasi-periods in SIC2 to SIC6 exhibit positive correlations with lags exceeding 12 months. This suggests a possible connection between ENSO and SIC variability at these points. The 1.7-year component of SIC1 shows a positive correlation with the 5.2-year AAOI index, while it exhibits a negative correlation ( $-0.51$ ) with the 2.2-year AAOI component.

Table III. Cross-correlation coefficients between the components of air temperature (Ta), sea surface temperature (SST), and sea ice cover (SIC) anomalies at reference points 1-6, and the components of the Antarctic Oscillation Index (AAOI) and Southern Oscillation Index (SOI) for the period 1981-2020.

Series	AAOI5.2	AAOI2.2	SOI3.5	SOI2.4
Ta1 4.4	0.52(1)	0.37(-3)	-0.41(16)	-0.30(11)
Ta1 1.0	-0.35(-6)	0.55 (0)		
Ta2 4.4	0.39(0)		-0.41(15)	
Ta2 1.1		-0.38		
Ta3 4.4	0.34(0)		-0.38(16)	
Ta3 1.3		-0.36(-6)		
Ta4 4.4	0.34(0)		-0.42(6)	
Ta4 1.1		-0.37(-6)		
Ta5 4.4	0.35(0)		-0.47(14)	-0.31(12)
Ta5 1.1		-0.35(-5)		
Ta6 4.4	0.53(0)	-0.31(6)	-0.47(14)	-0.33(11)
Ta6 2.4	-0.41(-10)	0.43(-3)	0.51(3)	-0.60(14)
Ta6 1.3	-0.34(-5)	0.51(0)		
SIC1 8.3		0.34(7)		
SIC1 3.1		0.43(7)		
SIC1 1.7	0.32(-6)	-0.51(0)		
SIC2 3.6			0.38(15)	
SIC3 4.4			0.35(17)	
SIC4 4.4			0.41(16)	
SIC5 4.4			0.40(15)	
SIC5 2.8			-0.32(6)	-0.36(4)
SIC6 4.4	-0.34(-1)		0.38(12)	
SIC6 2.0				0.36(18)
SST1 1.7	-0.31(10)			
SST5 4.6			-0.41(15)	
SST5 1.5		-0.33(14)		
SST6 5.2	0.30(-1)		0.47(-5)	

Lag months are indicated in parentheses.

## 5. Discussion

When analyzing the anomalies and extreme events of climatic parameters and indices, it is evident that the dominant climatic variability phenomenon affecting Ta in the WAP region is the SAM. This is reflected in the AAOI index, whose peak value occurred in May 1989, coinciding with most of the extreme absolute Ta events at the reference points. This can be explained by the positive phase of the SAM, which is characterized by anomalously lower air pressure over the Antarctic continent's center, combined with anomalously higher pressure over mid-latitudes. As a result, the Subpolar Front shifts southward, facilitating the influx of warmer air into

the Antarctic region and contributing to increased Ta in the WAP. Additionally, in July 1989, the SOI index was positive, indicating La Niña conditions. The simultaneous positive phases of both the AAOI and SOI likely amplified their combined impact, leading to the extreme warm Ta event.

The extreme cold Ta event occurred in July 1987 at all reference points. During this period, SOI was negative, indicating that ENSO was in its El Niño phase, while the AAOI was also negative. In the negative phase of the SAM, high atmospheric pressure is centered over the Antarctic continent, shifting the Subpolar Front northward and allowing colder air from higher latitudes to penetrate the

peninsula. The simultaneous negative phases of both the SOI and AAOI may have amplified their combined influence, potentially contributing to this extreme cold event.

This relationship is also evident in the statistical analysis, as shown by the cross-correlation results between the  $T_a$  series. The positive and moderate correlation between the 4.4-year component in all air temperature series and the 5.2-year AAOI index suggests that  $T_a$  variations with a 4.4-year cycle are linked to similar oscillations in the AAOI. Furthermore, the absence of lag indicates that this relationship is direct and synchronized.

Additionally, a positive relationship with the SOI is observed only at P6, the northernmost of the analyzed locations. In contrast, the other reference points reveal a negative relationship and a significant lag. This pattern may be explained by the influence of ENSO on the low-pressure system in the Amundsen Sea. In certain regions of Antarctica, during El Niño, when pressure in the Amundsen Sea is higher than usual, surface winds shift from northwest to southeast, transporting warm, moist air from the ocean towards the western Antarctic. Conversely, during La Niña, the pressure in the Amundsen Sea decreases, causing winds to blow from southeast to northwest, bringing drier and colder air (Raphael et al., 2016).

Regarding the SIC anomalies, in July 1995, the AAOI reached a minimum, and that same year, the maximum SIC was recorded at Point 6. The 3.5-year component of SOI exhibits positive correlations with the 3.6- and 4.4-year quasi-periods of SIC in most of the analyzed points, with lags exceeding 12 months. This indicates that SIC variability with a 3.5-year cycles is linked to oscillations in ENSO, suggesting that changes in ENSO may influence SIC with a prolonged time lag. Stammerjohn et al. (2008) associated SIC variations in the WAP with decadal ENSO changes in the SAM, which was negative in the 1980s and positive in the 1990s. They observed a significant response at high latitudes to ENSO, noting a stronger influence of ENSO when the SAM was negative during El Niño and when it was positive during La Niña. Additionally, SIC at P1 and P2 showed a significant decrease in 2008. That year, the AAOI and SOI indices were both in their positive phases. This suggests that the simultaneous positive phases of SOI and AAOI amplify their effects on SIC.

During El Niño events, the rise in Pacific Ocean temperatures can alter atmospheric circulation, bringing warmer and wetter air to the region, which may accelerate sea ice melting and reduce its coverage. In contrast, during La Niña, cooler Pacific temperatures can result in colder and drier winds over the Antarctic Peninsula, potentially promoting ice formation and increasing its extent. However, this holds only when considering atmospheric circulation alone, without accounting for the role of ocean processes. Aylmer et al. (2022) argue that sea ice loss in Antarctica is primarily driven by basal melting, with no direct atmospheric influence. Therefore, it is essential to examine how sea ice responds to oceanic dynamics, including feedback mechanisms. In this context, Si et al. (2023) highlight that low-resolution global models have yielded contradictory findings about the impact of additional meltwater on heat transport to the Antarctic continental shelf. Their results indicate that coastal cooling enhances heat flow toward the coast, implying a positive feedback loop in a warming climate. In other words, increased meltwater input could amplify heat transport to the coast, further accelerating ice shelf melting.

Additionally, analyzing SST anomalies is essential, as they may directly influence sea ice cover and support the hypothesis that basal sea ice melting is driven by oceanic heat. Most reference points reported a warm extreme in January 2017. Although no strong correlations were found between the SST series and the SOI or AAOI (Table II), this could be explained by heat advection from ocean currents, which needs to be further examined. In the decomposition and cross-correlation analysis, the AAOI5.2 shows a negative correlation with the 1.7-year component of SST1, with a large lag and a positive correlation with the 5.2-year component of SST6. According to Damini et al. (2022), deep water masses in the Bransfield Strait display marked interannual variability in their thermohaline properties, primarily driven by ENSO and SAM. Furthermore, Evtushevsky et al. (2015) note that SST anomalies in the central tropical Pacific, specifically near the Niño-4 region, serve as a key indicator of tropical convection strength and influence the generation of planetary waves. These waves, particularly the quasi-stationary wave number 1, can propagate from the troposphere to the Antarctic

stratosphere, establishing teleconnections between tropical regions and the polar stratosphere of the Southern Hemisphere.

The distinct behavior of P1, located in the Bransfield Strait, compared to the other points, is also explained by Moffat and Meredith (2018), who argue that variability in bathymetry and the differing influences of waters from the ACC and the Weddell Sea in the Bransfield Strait and the central region of the WAP create a strong hydrographic gradient along the coast. Additionally, they maintain that the steep slope of the Bransfield Strait and the relatively shallow bathymetry around the islands at its boundary with the central WAP likely inhibit the exchange of water properties between these two regions.

The correlations between SST at P5 (4.6-year quasi-period) and P6 (5.2-year quasi-period) with the SOI3.5 indicate an influence of ENSO dynamics on regional SST variability. This aligns with Damini et al. (2022), who highlight how ENSO-driven changes in wind patterns and ocean currents further influence the intrusion of deep waters, particularly CDW, into the Antarctic Peninsula region.

## 6. Conclusions

The absolute extreme Ta and SST events in the WAP region are strongly influenced by the SAM and ENSO. In most cases, the extreme positive Ta anomaly in July 1989 and the extreme negative Ta anomaly in July 1987 reflect the in-phase behavior of the SAM and ENSO oscillations, which modulate the inflow of warm or cold air into the region. When SOI and AAOI are in the negative (positive) phase, Ta reaches a negative (positive) absolute extreme.

The positive and moderate correlation between the 4.4-year components of air temperature and the 5.2-year AAOI indicates synchronization between these cycles. The combination of a negative SOI (El Niño) and negative AAOI is associated with positive absolute extremes of Ta and SST, and with reduced sea ice concentration in the western Antarctic Peninsula.

The 3.5-year cycles of the SOI index, showing positive correlations and significant lags with the SIC series, highlight the influence of ENSO on sea ice variability in the Antarctic Peninsula. This suggests that ENSO-related atmospheric and oceanic changes modulate sea ice coverage over multi-year timescales.

The dominant SST cycles in the WAP region include components of approximately 1.7, 4.4, and 5.2 years, reflecting the complex interactions between oceanic circulation and climate patterns. SST variations are linked to changes in heat transport and the advection of deep waters, modulated by ENSO and SAM phases.

Variability in the Bransfield Strait exhibits a unique behavior due to the influence of bathymetry and the interaction of waters from the ACC and the Weddell Sea. The phases of SAM and ENSO modulate the transport of deep waters into the strait. Opposite-phase combinations of SOI and AAOI (e.g., El Niño with positive SAM) may weaken each other's influence on regional climate conditions.

The results highlight the significant influence of ENSO and SAM on extreme events and multi-year variability in Ta, SST, and SIC in the WAP. However, the complexity of these interactions suggests the need for further research incorporating additional atmospheric and oceanic variables, such as wind stress, ocean heat content, and regional circulation patterns. Future studies could also explore the role of other climate modes, as well as the potential non-linear interactions between ENSO, SAM, and local ocean-atmosphere dynamics, to improve predictive capabilities and refine our understanding of climate variability in the Antarctic Peninsula.

## References

- Aylmer J, Ferreira D, Feltham D. 2022. Different mechanisms of Arctic and Antarctic sea ice response to ocean heat transport. *Climate Dynamics* 59: 315-329. <https://doi.org/10.1007/s00382-021-06131-x>
- Balmaseda MA, Mogensen K, Weaver AT. 2013. Evaluation of the ECMWF ocean reanalysis system ORAS4. *Quarterly Journal of the Royal Meteorological Society* 139: 1132-1161. <https://doi.org/10.1002/qj.2063>
- Bozkurt D, Bromwich DH, Carrasco J, Hines KM, Maureira JC, Rondanelli R. 2020. Recent near-surface temperature trends in the Antarctic Peninsula from observed, reanalysis and regional climate model data. *Advances in Atmospheric Sciences* 37: 477-493. <https://doi.org/10.1007/s00376-020-9183-x>
- Cook AJ, Holland PR, Meredith MP, Murray T, Luckman A, Vaughan DG. 2016. Ocean forcing of glacier retreat in the western Antarctic Peninsula. *Science* 353: 283-286. <https://doi.org/10.1126/science.aae0017>

- Damini BY, Kerr R, Dotto TS, Mata MM. 2022. Long-term changes on the Bransfield Strait deep water masses: Variability, drivers and connections with the northwestern Weddell Sea. *Deep Sea Research Part I: Oceanographic Research Papers* 179: 103667. <https://doi.org/10.1016/j.dsr.2021.103667>
- Domack E, Levente A, Burnet A, Bindschadler R, Convey P, Kirby M. 2003. Antarctic Peninsula climate variability: Historical and paleoenvironmental perspectives. Vol. 79. American Geophysical Union. <https://doi.org/10.1029/AR079>
- Dotto TS, Kerr R, Mata MM, García CAE. 2016. Multidecadal freshening and lightening in the deep waters of the Bransfield Strait, Antarctica. *Journal of Geophysical Research: Oceans* 121: 3741-3756. <https://doi.org/10.1002/2015JC011228>
- Evtushevsky OM, Kravchenko VO, Hood LL, Milinevsky GP. 2015. Teleconnection between the central tropical Pacific and the Antarctic stratosphere: Spatial patterns and time lags. *Climate Dynamics* 44: 1841-1855. <https://doi.org/10.1007/s00382-014-2375-2>
- Evtushevsky O, Grytsai A, Agapitov O, Kravchenko V, Milinevsky G. 2021. The 16-year periodicity in the winter surface temperature variations in the Antarctic Peninsula region. *Climate Dynamics* 58: 35-47. <https://doi.org/10.1007/s00382-021-05886-7>
- Fogt RL, Marshall GJ. 2020. The Southern Annular Mode: Variability, trends, and climate impacts across the Southern Hemisphere. *Wiley Interdisciplinary Reviews: Climate Change* 11: e652. <https://doi.org/10.1002/wcc.652>
- Hernández Duarte MA, Villegas Bolaños NL, Concha Perdomo AE. 2021. Descripción general de algunas variables meteo-marinas de aguas superficiales adyacentes al archipiélago de Palmer, península Antártica, durante 1979-2018 con base en datos ERA5. *Bulletin of Marine and Coastal Research* 50: 141-162. <https://doi.org/10.25268/bimc.invemar.2021.50.1.968>
- Hersbach H, Bell B, Berrisford P, Hirahara S, Horányi A, Muñoz-Sabater J, Nicolas J, Peubey C, Radu R, Schepers D, Simmons A, Soci C, Abdalla S, Abellan X, Balsamo G, Bechtold P, Biavati G, Bidlot J, Bonavita M, De Chiara G, Dahlgren P, Dee D, Diamantakis M, Dragani R, Flemming J, Forbes R, Fuentes M, Geer A, Haimberger L, Healy S, Hogan RJ, Hólm E, Janisková M, Keeley S, Laloyaux P, Lopez P, Lupu C, Radnoti G, de Rosnay P, Rozum I, Vamborg F, Villaume S, Thépaut J-N. 2020. The ERA5 global reanalysis. 2020. *Quarterly Journal of the Royal Meteorological Society* 146: 1999-2049. <https://doi.org/10.1002/qj.3803>
- Houser C, Smith A, Wernette P, Lehner J. 2022. Spatial frequency analysis and information synthesis for understanding coastal barriers. In: *Treatise on geomorphology*. Vol. 1: Technology-driven geomorphology: Geospatial data science (Bishop MP, Giardino JR, Eds.). Elsevier, 169-204. <https://doi.org/10.1016/B978-0-12-818234-5.00023-7>
- Meredith MP, Murphy EJ, Hawker EJ, King JC, Wallace MI. 2008. On the interannual variability of ocean temperatures around South Georgia, Southern Ocean: Forcing by El Niño/Southern Oscillation and the Southern Annular Mode. *Deep Sea Research Part II: Topical Studies in Oceanography* 55: 2007-2022. <https://doi.org/10.1016/j.dsr2.2008.05.020>
- Moffat C, Meredith M. 2018. Shelf-ocean exchange and hydrography west of the Antarctic Peninsula: A review. *Philosophical Transactions of the Royal Society A, Mathematical, Physical and Engineering Sciences* 376: 20170164. <https://doi.org/10.1098/rsta.2017.0164>
- Morris EM, Vaughan DG. 2003. Spatial and temporal variation of surface temperature on the Antarctic Peninsula and the limit of viability of ice shelves. In: *Antarctic Peninsula climate variability: Historical and paleoenvironmental perspectives* (Domack E, Levente A, Burnet A, Bindschadler R, Convey P, Kirby M, Eds.). American Geophysical Union, 61-68. <https://doi.org/10.1029/AR079p0061>
- NOAA-CPC. 2023. Climate indices: Monthly atmospheric and ocean time series. National Oceanic and Atmospheric Administration-Climate Prediction Center. Available at: <https://psl.noaa.gov/data/climateindices/list/> (accessed 2024 October 23)
- Pohl B, Fauchereau N, Reason CJC, Rouault M. 2010. Relationships between the Antarctic Oscillation, the Madden-Julian oscillation, and ENSO, and consequences for rainfall analysis. *Journal of Climate* 23: 238-254. <https://doi.org/10.1175/2009JCLI2443.1>
- Raphael MN, Marshall GJ, Turner J, Fogt RL, Schneider D, Dixon DA, Hosking JS, Jones JM, Hobbs WR. 2016. The Amundsen Sea Low: Variability, change, and impact on Antarctic climate. *Bulletin of the American Meteorological Society* 97: 111-121. <https://doi.org/10.1175/BAMS-D-14-00018.1>
- Ruiz Barlett EM, Tosonotto GV, Piola AR, Sierra ME, Mata MM. 2018. On the temporal variability of intermediate and deep waters in the western basin of the

- Bransfield Strait. *Deep Sea Research Part II: Topical Studies in Oceanography* 149: 31-46. <https://doi.org/10.1016/j.dsr2.2017.12.010>
- Si Y, Stewart AL, Eisenman I. 2023. Heat transport across the Antarctic Slope Front controlled by cross-slope salinity gradients. *Science Advances* 9: eadd7049. <https://doi.org/10.1126/sciadv.add7049>
- Spence P, Griffies SM, England MH, Hogg AM, Saenko OA, Jourdain NC. 2014. Rapid subsurface warming and circulation changes of Antarctic coastal waters by poleward shifting winds. *Geophysical Research Letters* 41: 4601-4610. <https://doi.org/10.1002/2014GL060613>
- Spence P, Holmes RM, Hogg AM, Griffies SM, Stewart KD, England MH. 2017. Localized rapid warming of West Antarctic subsurface waters by remote winds. *Nature Climate Change* 7: 595-603. <https://doi.org/10.1038/nclimate3335>
- Stammerjohn SE, Martinson DG, Smith RC, Yuan X, Rind D. 2008. Trends in Antarctic annual sea ice retreat and advance and their relation to El Niño-Southern Oscillation and Southern Annular Mode variability. *Journal of Geophysical Research: Oceans* 113: C03S90 <https://doi.org/10.1029/2007JC004269>
- StatSoft. 2007. *Statistica* (data analysis software system), v. 8. Available at [www.statsoft.com](http://www.statsoft.com) (accessed 2024 October 23).
- Stenni B, Curran MAJ, Abram NJ, Orsi A, Goursaud S, Masson-Delmotte V, Neukom R, Goosse H, Divine D, Van Ommen T, Steig EJ, Dixon DA, Thomas ER, Bertler NAN, Isaksson E, Ekaykin A, Werner M, Frezzotti M. 2017. Antarctic climate variability on regional and continental scales over the last 2000 years. *Climate of the Past* 13: 1609-1634. <https://doi.org/10.5194/cp-13-1609-2017>
- Suryawanshi K, Jena B, Bajish CC, Anilkumar N. 2023. Recent decline in Antarctic sea ice cover from 2016 to 2022: Insights from satellite observations, argo floats, and model reanalysis. *Tellus A: Dynamic Meteorology and Oceanography*. <https://doi.org/10.16993/tellusa.3222>
- Turner J, Marshall GJ, Clem K, Colwell S, Phillips T, Lu H. 2019. Antarctic temperature variability and change from station data. *International Journal of Climatology* 40: 2986-3007. <https://doi.org/10.1002/joc.6378>
- Villegas N, Malikov I. 2020. Análisis Espectral Correlación y Pronóstico AECPA (ARIMA), v. 0.23.03.01. Available at <https://github.com/glignan/AECPA/releases/tag/v.0.23.03.01> (accessed 2024 October 23).
- Von Gyldenfeldt AB, Fahrbach E, García MA, Schröder M. 2002. Flow variability at the tip of the Antarctic Peninsula. *Deep Sea Research Part II: Topical Studies in Oceanography* 49: 4743-4766. [https://doi.org/10.1016/S0967-0645\(02\)00157-1](https://doi.org/10.1016/S0967-0645(02)00157-1)
- Wang X, Moffat C, Dinniman MS, Klinck JM, Sutherland DA, Aguiar-González B. 2022. Variability and dynamics of along-shore exchange on the West Antarctic Peninsula (WAP) continental shelf. *Journal of Geophysical Research: Oceans* 127: e2021JC017645 <https://doi.org/10.1029/2021JC017645>
- Ward JH. 1963. Hierarchical grouping to optimize an objective function. *Journal of the American Statistical Association* 58: 236-244. <https://doi.org/10.1080/01621459.1963.10500845>
- Wu Q, Zhang X, Church JA, Hu J. 2019. ENSO-related global ocean heat content variations. *Journal of Climate* 32: 45-68. <https://doi.org/10.1175/JCLI-D-17-0861.1>